(0.46-cm²) disk electrode was employed as the working electrode. Rotating ring–disk experiments were conducted using a RDE4 instrument (Pine Instrument Company). A pyrolytic graphite disk/platinum ring electrode was used. The ring collection efficiency ($N = 0.17$) was determined using a solution of ferrocene. All working electrode surfaces were highly polished with alumina paste prior to each experiment. Adsorption of metalloporphyrins was accomplished by dropping organic solvents containing metalloporphyrins on the disk electrode, followed by careful evaporation of the solvent. Aqueous solutions of water-soluble porphyrins were prepared using distilled–deionized water with less than 0.5% *N,N*-dimethylformamide (DMF). Dioxygen concentrations in O_2-saturated solutions were assumed to be 1.2 mM at room temperature. Solutions of 0.1 N H_2SO_4 were used as supporting electrolytes. All reported potentials are with respect to a saturated calomel electrode (SCE).

Theoretical Calculations. All model building and calculations were performed on a Silicon Graphics IRIS 4D/220 GTX workstation, using the programs Quanta version 3.2 (Polygen Corp.) and CHARM$_m$[3] version 21.2. The topology file PORPHYRINH.RTF supplied by Polygen was used as a basis for the porphyrin moieties of the dimers, and the linkers were constructed in Chemnote, the 2D modeling facility in Quanta. Minimizations were performed using the steepest descent algorithm, followed by an adopted basis Newton–Raphson algorithm, until the energy change tolerance was less than 10^{-9} kcal/mol. The nonbonded interaction cutoff distance and hydrogen bonding cutoff distance were chosen to be 11.5 and 7.5 Å, respectively. Molecular dynamics were performed using Verlet integration and the SHAKE algorithm to fix C–H bonds. At 600 K, the maximum allowable fluctuation in temperature was fixed at 25 K. Nonbonded interaction and hydrogen bond lists were updated every 0.05 ps.

Preparation of Co_2-1. A mixture of **1**[9] (20 mg, 0.0102 mmol) and $CoCl_2 \cdot 6H_2O$ (100 mg, 0.42 mmol) was heated at 135 °C for 5 h and then diluted with chloroform (100 mL) and methanol (25 mL). The reaction mixture was extracted with 5% aqueous ammonium hydroxide solution, water, and brine, and the organic layer was separated, dried over anhydrous Na_2SO_4, filtered, and evaporated to give 19 mg (90.4%) of Co_2-**1** as a deep orange powder: FABMS m/z 2071 (calcd for $C_{116}H_{80}N_{16}O_8S_4Co_2$ [M^+] m/z 2070.5); UV/vis (DMF) λ_{max} ($\epsilon \times 10^{-3}$ cm^{-1} M^{-1}) 409 (121), 529 (17.7).

Preparation of Co_2-2. A mixture of **2**[9] (10 mg, 0.0049 mmol) and $CoCl_2 \cdot 6H_2O$ (50 mg, 0.21 mmol) in DMF (5 mL) was heated at 135 °C for 6 h. The reaction mixture was evaporated, and the resulting green residue was triturated with cold water, filtered, washed with ether, and dried to give 9.8 mg (93.3%) of Co_2-**2** as a deep orange powder: FABMS m/z 2115 (calcd for $C_{119}H_{89}N_{16}O_8S_4Co_2$ [$M^+ - CH_3$] m/z 2115.5); UV/vis (DMF) λ_{max} ($\epsilon \times 10^{-3}$ cm^{-1} M^{-1}) 409 (300), 530 (28.3).

Preparation of Co_2-3. A mixture of **3**[9] (10 mg, 0.0064 mmol) and $CoCl_2 \cdot 6H_2O$ (50 mg, 0.21 mmol) in DMF (20 mL) was heated at 120 °C for 48 h. The reaction mixture was evaporated to dryness, and the reddish residue was triturated with water (100 mL × 3), collected, washed with ether, and dried at 25 °C/0.2 mmHg to give 9.2 mg (85.7%) of Co_2-**3** as a reddish powder: FABMS m/z 1678 (calcd for $C_{100}H_{72}N_{16}O_4Co_2$ (M^+) m/z 1678.5); UV/vis (DMF) λ_{max} ($\epsilon \times 10^{-3}$ cm^{-1}) 409 (267), 529 (17.8).

Preparation of Co_2-4. A mixture of **4**[9] (18 mg, 0.012 mmol) and $CoCl_2 \cdot 6H_2O$ (50 mg, 0.21 mmol) in DMF (10 mL) was heated at 95 °C for 8 h and then diluted with chloroform (100 mL). The reaction mixture was extracted with water and brine, dried over anhydrous Na_2SO_4, filtered, and evaporated to yield a deep orange powder. The resulting orange residue was subjected to silica gel column eluting with a mixture of chloroform/methanol (100:3). The nonpolar orange band was collected to give 17 mg (87.6%) of Co_2-**4** as a deep orange powder: UV/vis ($CHCl_3$) λ_{max} ($\epsilon \times 10^{-3}$ cm^{-1} M^{-1}) 406 (320), 530 (27.7); FABMS m/z 1607 (calcd for $C_{100}H_{64}N_{16}Co_2$ [M^+] m/z 1606.4).

Preparation of Co_2-6. A mixture of **6**[9] (10 mg, 0.0054 mmol) and $CoCl_2 \cdot 6H_2O$ (50 mg, 0.21 mmol) in DMF (30 mL) was heated at 120 °C for 48 h and then diluted with chloroform (200 mL). The reaction mixture was extracted with water and brine, dried over anhydrous Na_2SO_4, filtered, and evaporated to yield 9.7 mg (91.5%) of Co_2-**6** as a deep orange powder: FABMS m/z 1974 (calcd for $C_{112}H_{76}N_{14}O_9S_3Co_2$ [M^+] m/z 1974.4); UV/vis (DMF) λ_{max} ($\epsilon \times 10^{-3}$ cm^{-1} M^{-1}) 410 (209), 530 (16.7).

Preparation of Co-8. A mixture of **8**[8b] (50 mg, 0.051 mmol), $CoCl_2 \cdot 6H_2O$ (100 mg, 0.42 mmol), and NaBr (1 g) in DMF (20 mL) was heated at 80 °C for 24 h and then diluted with chloroform (200 mL). The reaction mixture was extracted with water and brine, and the organic layer was separated, dried over anhydrous Na_2SO_4, filtered, and evaporated to yield an orange powder. The resulting orange residue was subjected to silica column eluting with a mixture of chloroform/methanol (100:3). The nonpolar band was collected to give 28 mg (53%) of Co-**8** as deep orange powder: UV/vis ($CHCl_3$) λ_{max} ($\epsilon \times 10^{-3}$ cm^{-1} M^{-1}) 410 (151), 528 (20.5); FABMS m/z 1039 (calcd for $C_{48}H_{32}Br_4N_4Co$ [M^+] m/z 1038.9).

Acknowledgment. This study was supported by grants from the National Institute of Health and Protos Corporation of Emeryville, CA.

Registry No. 1, 134260-60-9; Co_2-**1**, 141090-89-3; **2**, 134209-10-2; Co_2-**2**, 141090-90-6; **3**, 138312-89-7; Co_2-**3**, 141090-91-7; **4**, 133672-00-1; Co_2-**4**, 141090-92-8; **5**, 133671-99-5; **6**, 138312-91-1; Co_2-**6**, 141090-93-9; **7**, 138312-92-2; **8**, 133671-91-7; Co-**8**, 141090-94-0; O_2, 7782-44-7.

(9) Karaman, R.; Blaskó, A.; Almarsson, Ö.; Arasasingham, R.; Bruice, T. C. *J. Am. Chem. Soc.*, preceding paper in this issue.

Communications to the Editor

An Alternate Geometry for the Catalytic Triad of Serine Proteases

David R. Corey,† Mary E. McGrath,‡ John R. Vásquez,† Robert J. Fletterick,*,‡ and Charles S. Craik*,†,‡

Department of Pharmaceutical Chemistry and Department of Biochemistry, University of California San Francisco, California 94143-0446

Received January 31, 1992

The catalytic triad of serine proteases, Asp–His–Ser, is one of the classic motifs of enzymology. Effective strategies for the incorporation of the triad into non-protease protein scaffolds (i.e., antibodies[1] or de novo designed peptides[2]) might allow the development of sequence-specific peptidases or other novel enzymes. Such catalyst design would be facilitated by knowledge of the limits within which the orientation or composition of the triad members can be altered while still preserving significant peptidase activity.

We have previously reported that, of the three members of the triad, only the serine in trypsin is necessary for a minimal level of catalysis toward peptide bonds.[3] In this communication we report the mutation of Asp 102 and the partial replacement of its function in catalysis through the introduction of aspartic or glutamic acid in place of a neighboring amino acid, Ser 214. The

*Authors to whom communication should be addressed.
†Department of Pharmaceutical Chemistry.
‡Department of Biochemistry.

(1) (a) Lerner, R. A.; Benkovic, S. J.; Schultz, P. G. *Science* **1991**, *252*, 659–667. (b) Lewis, C. T.; Hilvert, D. *Curr. Opin. Struct. Biol.* **1991**, *1*, 624–629.

(2) (a) DeGrado, W. F.; Wasserman, Z. R.; Lear, J. D. *Science* **1989**, *243*, 622–628. (b) Hahn, K. W.; Klis, W. A.; Stewart, J. M. *Science* **1990**, *248*, 1544–1547. (c) Sander, C. *Curr. Opin. Struct. Biol.* **1991**, *1*, 630–637. (d) DeGrado, W. F.; Raleigh, D. P.; Handel, T. *Curr. Opin. Struct. Biol.* **1991**, *1*, 984–993.

(3) Corey, D. R.; Craik, C. S. *J. Am. Chem. Soc.* **1992**, *114*, 1784–1790.

0002-7863/92/1514-4905$03.00/0

Table I. Kinetic Parameters for Triad Variants toward Z-GPR-AMC and Insulin β-Chain[a]

substrate	variant	k_{cat} (min^{-1})	K_m (μM)	k_{cat}/K_m	k_{cat}/K_m wt/mut	k_{cat} wt/mut
Z-GPR-AMC	wild type	4100	16	256	1	1
	D102S/S214D	13	9.7	1.3	196	315
	D102S/S214E	570	1700	0.34	753	7.2
	D102S	1	50	0.02	12800	4100
insulin β-chain	wild type	2500	140	18	1	1
	D102S/S214D	42	560	0.075	240	60
	D102S/S214E	26	2000	0.013	1385	96
	D102S	0.06	30	0.002	9000	41700

[a] The error in determinations using Z-R-AMC or Z-GPR-AMC was 10–20%. The error in determinations using insulin β-chain was 20–30%. The buffer was 100 mM NaCl, 20 mM $CaCl_2$, and 50 mM Tris-Cl, pH 8.0.

mutations D102S, D102S/S214E, and D102S/S214D were introduced into the gene coding for rat anionic trypsin via site-directed mutagenesis,[4] and the corresponding mutant proteins were expressed in *Escherichia coli*.[3]

Assays toward the activated amide substrate, benzyloxycarbonyl-Gly-Pro-Arg-7-amido-4-methylcoumarin (Z-GPR-AMC), showed that the k_{cat}/K_m for each mutant was much reduced relative to the wild type (0.5–0.01%) (Table I). However, we noted that the D102S/S214E mutant had a nearly 600-fold-higher turnover number than the analogous single mutant D102S, suggesting that E214 was assuming a role in catalysis. The much higher K_m of the D102S/S214E protein is likely due to a gross alteration in the orientation of the indole side chain of Trp 215. This distortion had previously been observed in the X-ray crystal structures of the single mutants S214E and S214K, which exhibit similar high K_m values.[5]

The variant proteins were then assayed for activity toward a more physiologically and chemically revealing substrate, insulin β-chain.[3,6] In contrast to the coumarin substrate Z-GPR-AMC, cleavage of insulin β-chain is indicative of the ability of the enzyme to hydrolyze unactivated amide bonds. k_{cat}/K_m for the D102S/S214E and the D102S/S214D mutants were 5.6- and 33-fold higher, respectively, than that for the D102S mutant (Table I). Most of this increase was due to dramatically enhanced k_{cat} values for the double mutants relative to the D102S mutant (724-fold higher for D102S/S214D, 446-fold higher for D102S/D214E). It is worth noting that the relatively high k_{cat} for the D102S/S214D mutant could not have been predicted on the basis of kinetic measurements with the activated coumarin substrate. In the case of the D102S/S214D enzyme, k_{cat}/K_m and k_{cat} reach 0.4% and 1.7% of those for the wild type, respectively, compared to 0.01% and 0.002% for the D102S single mutant.

The k_{cat} for trypsin D102S/S214D actually *increases* for the hydrolysis of the less labile amide linkage of insulin β-chain relative to the activated amide-containing coumarin substrate (42 min^{-1} vs 13 min^{-1}).[7] To examine the structural origins of this differential reactivity, trypsin D102S/S214D was crystallized in the presence of the small molecule inhibitor benzamidine. This ground-state structure was determined to 2.25-Å resolution as described previously for other mutants.[8] The variant was found to be structurally similar to trypsin except at the two sites of mutation (102, 214) and at the other triad residues (His 57, Ser 195). In contrast to the rotated Trp 215 in the S214E and S214K structures, Trp 215 was not displaced.

Two salient features of the crystal structure are worth noting: (1) Asp 214 is in an anti orientation for hydrogen bonding to histidine rather than the preferred syn conformation in which the histidine is bifurcated by the carboxylate oxygens (Figure 1).[9]

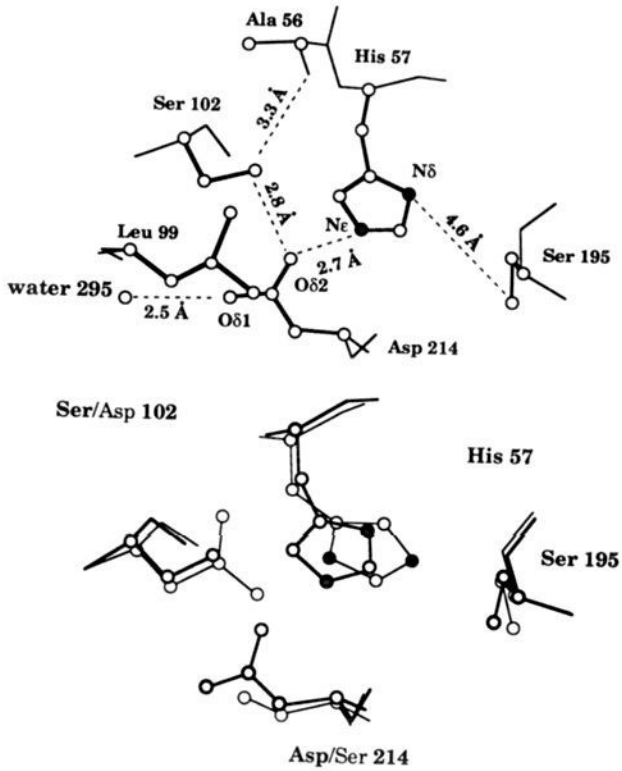

Figure 1. Top: A MacImdad (Molecular Applications Group, Stanford, CA) drawing of the refined coordinates of the active site of trypsin D102S/S214D shown with the His 57 imidazolium nitrogens labeled and shaded. The hydrogen bonds and distances of interest are identified. Leu 99 is a surface residue whose side chain is responsible, in part, for the solvent inaccessibility of the amino acids at positions 102 and 214. Bottom: A MacImdad drawing of the active sites of trypsin and trypsin D102S/S214D shown superimposed by Cα. Trypsin D102S/S214D, which features Ser 102, His 57, Ser 195, and Asp 214, is represented in thick lines, while trypsin is shown in thin lines. Note that trypsin His 57 Nε2 forms a long hydrogen bond with Ser 195 Oγ, while in trypsin D102S/S214D His 57 Nδ1 is the proximal nitrogen.

This alone might decrease k_{cat} by 10^2–10^4-fold.[9a] (2) The imidazole of His 57 was rotated 180° approximately (χ_2 from −102° to 91°) relative to wild-type trypsin. His 57 retreats 1 Å from Ser 195 toward the introduced aspartic acid at 214 to form a strong hydrogen bond with it. This moves the proton acceptor for Ser 195 OγH, now Nδ of His 57 instead of Nε, about 1.5 Å further away from Oγ. Presumably Ser 195 and His 57 alter their configurations upon substrate binding, since otherwise the Ser 195 proton would have to traverse a distance of 4.6 Å between Ser 195 Oγ and Nδ of His 57[10] during catalysis.

The seemingly unfavorable geometry of the serine and histidine suggested that the trypsin D102S/S214D–benzamidine structure could not represent the configuration responsible for the high k_{cat} toward insulin β-chain relative to the tripeptide activated amide substrate Z-GPR-AMC. Presumably, binding the extended peptide of insulin β-chain filled the S1′, S2′, and S3′ subsites on the surface of trypsin and reconfigured the enzyme active site into a better orientation for catalysis. Small inhibitors like benzamidine, which do not fill these subsites, would be unable to induce this reorganization.

Trypsins which lack a catalytic carboxylate at position 102 can be reconstituted by the introduction of a carboxylate elsewhere.

(4) Kunkel, T. A. *Proc. Natl. Acad. Sci. U.S.A.* **1985**, *82*, 488–492.
(5) McGrath, M. E.; Vasquez, J. R.; Craik, C. S.; Yang, A. S.; Honig, B.; Fletterick, R. J. *Biochemistry* **1992**, *31*, 3059–3064.
(6) Hua, Q. X.; Shoelson, S. E.; Kochoyan, M.; Weiss, M. A. *Nature* **1991**, *254*, 238–241.
(7) The decrease in k_{cat} for the D102S/S214E mutant toward insulin β-chain relative to Z-GPR-AMC (26 vs 570) may be related to the high K_m for substrate.
(8) McGrath, M. E.; Wilke, M. E.; Higaki, J. N.; Craik, C. S.; Fletterick, R. J. *Biochemistry* **1989**, *28*, 9264–9270.
(9) (a) Gandour, R. D. *Bioorg. Chem.* **1981**, *10*, 169–176. (b) Huff, J. B.; Askew, B.; Duff, R. J.; Rebek, J. *J. Am. Chem. Soc.* **1988**, *110*, 5908–5909. (c) Cramer, K. D.; Zimmerman, S. C. *J. Am. Chem. Soc.* **1990**, *112*, 3680–3682.
(10) For example, Ser 195 is seen to rotate about 1.0 Å closer to His 57 on binding to bovine pancreatic trypsin inhibitor (BPTI). It can be seen by modeling that this structural adjustment in trypsin D102S/S214D would reposition the Ser 195 Oγ to ~3.8 Å from Nδ of His 57. Perona, J. J.; Tsu, C.; McGrath, M. E.; Craik, C. S.; Fletterick, R. J. Unpublished data.

Kinetic and structural data reaffirm the importance of the buried negative charge adjacent to His 57,[11,12] but suggest that its absolute position is critical only for the highly efficient catalysis of the wild-type enzyme. Therefore, in spite of the observation that the active sites of the structurally unrelated enzymes of the trypsin and subtilisin families have converged to geometries with less than a 0.2-Å root mean square deviation,[13] designed proteins which are meant to incorporate serine protease-like activity can utilize an alternate orientation for the carboxylate. The flexibility inherent in these alternate motifs may facilitate the introduction of efficient catalytic triads into other scaffolds without disruption of preexisting substrate binding or catalysis.

Acknowledgment. This work was supported by NSF Grants DMB-8904956 and EET-8807179 to C.S.C., NIH Grant DK39304 to R.J.F., and a Damon Runyon-Walter Winchell Fellowship to D.R.C. (DRG 1076).

(11) (a) Craik, C. S.; Roczniak, S.; Largman, C.; Rutter, W. J. *Science* **1987**, *237*, 909–913. (b) Sprang, S.; Standing, T.; Fletterick, R. J.; Stroud, R. M.; Finer-Moore, J.; Xuong, N.-H.; Hamlin, R.; Rutter, W. J.; Craik, C. S. *Science* **1987**, *237*, 905–909.
(12) Warshel, A.; Russell, S. *J. Am. Chem. Soc.* **1986**, *108*, 6569–6579.
(13) (a) Garavito, R. M.; Rossman, M. G.; Argos, P.; Eventoff, W. *Biochemistry* **1977**, *16*, 5065–5071 and references therein. (b) Craik, C. S.; Fletterick, R. S. Unpublished data.

Extraframework Sodium Cation Sites in Sodium Zeolite Y Probed by ^{23}Na Double-Rotation NMR

Raz Jelinek

Materials Sciences Division, Lawrence Berkeley Laboratory and Department of Chemistry University of California, Berkeley, California 94720

Saim Özkar† and Geoffrey A. Ozin*

Advanced Zeolite Materials Science Group Lash Miller Chemical Laboratories University of Toronto, 80 Saint George Street Toronto, Ontario, Canada M5S 1A1

Received December 2, 1991

The most commonly encountered "inorganic" charge-balancing cation found in as-synthesized zeolites is Na^+. Extraframework Na^+ cations play an important role in determining the adsorption, chemical, catalytic, and solid-state properties of zeolites with respect to a wide range of guests.[1,2] ^{23}Na NMR spectra, however, usually exhibit large quadrupolar broadening even upon magic angle spinning (MAS), which renders the interpretation of the experimental data difficult.[3] The newly developed double-rotation (DOR) technique removes the anisotropic broadening of quadrupolar nuclei, thereby facilitating significantly improved spectral resolution.[4] We report here for the first time high-resolution ^{23}Na DOR spectra of dehydrated sodium zeolite Y, $Na_{56}Y$, and its Tl^+ exchanged derivatives, $Tl_nNa_{56-n}Y$.[5] By interchanging Tl^+ and Na^+ cations at particular locations within the unit cell of $Na_{56}Y$,[6] we are able to identify distinct ^{23}Na DOR signals which correspond to Na^+ cations at specific sites, as well as deduce some information concerning the ion-exchange pathway.

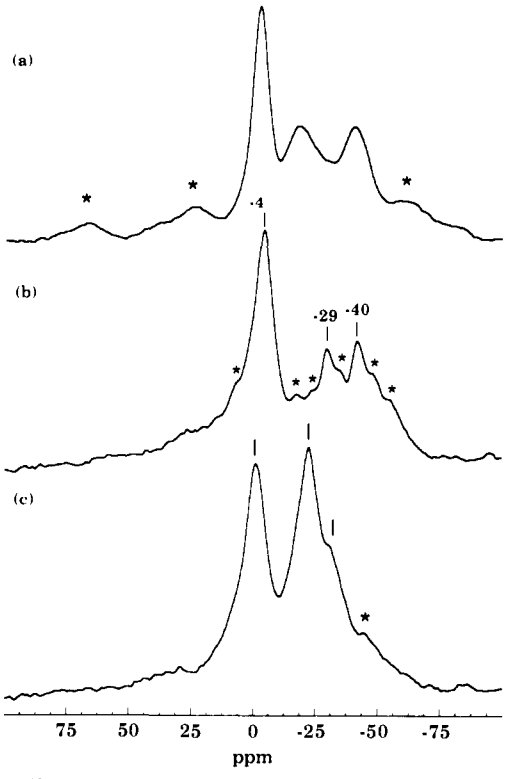

Figure 1. ^{23}Na NMR spectra of $Na_{56}Y$ zeolite: (a) MAS spectrum of dehydrated $Na_{56}Y$; (b) DOR spectrum of dehydrated $Na_{56}Y$; (c) DOR spectrum of $16\{W(CO)_6\}$-$Na_{56}Y$. * indicates spinning side bands.

^{23}Na NMR spectra of dehydrated $Na_{56}Y$ are shown in Figure 1. The MAS spectrum, Figure 1a, displays a peak around −4 ppm, while features upfield are composed of quadrupolar broadened peaks and overlapping spinning side bands. The DOR spectrum, shown in Figure 1b, yields higher resolution. The anisotropic quadrupolar broadening is averaged out in the DOR experiment, and three distinct peaks emerge: a prominent Gaussian around −4 ppm and two weaker peaks, on top of a broad background signal and a side band manifold, at −29 ppm and −40 ppm, respectively.

In order to assign the ^{23}Na DOR signals to specific Na^+ sites within the zeolite lattice, we first examined the spectrum of $16\{W(CO)_6\}$-$Na_{56}Y$, shown as Figure 1c. An intense resonance is observed around −26 ppm. This peak is assigned to Na^+ cations at site II in the α-cage, since previous studies have determined that an α-cage-encapsulated $W(CO)_6$ molecule is anchored to two site II Na^+ cations.[8]

XRD and ND measurements[9] establish that about 7–8% of the Na^+ cations in dehydrated $Na_{56}Y$ occupy site I, 24–33% are located inside the β-cage at site I′, 53–57% are inside the α-cage at site II, and the remainder are either in the α-cage at site III or unlocated. The distribution of Na^+ cations seems different from that which we observe in the DOR experiment. The relatively small intensity of the ^{23}Na DOR resonance from site II Na^+ in the virgin dehydrated $Na_{56}Y$, at around −30 ppm (Figure 1b), might originate from a distribution of chemical environments of Na^+ at this site, which could also explain the broad background ^{23}Na signal. This distribution might be brought about through motion, on the time scale of the NMR experiment, of the site II

* To whom correspondence should be addressed.
† Chemistry Department, Middle East Technical University, Ankara, Turkey, 06531.

(1) Breck, D. W. *Zeolite Molecular Sieves*; R. E. Kieger Publishing Company: Malabar, 1984.
(2) Ozin, G. A.; Stein, A.; Kuperman, A. *Angew. Chem., Int. Ed. Engl.* **1989**, *101*, 373.
(3) Engelhardt, G. In Introduction to Zeolite Science and Practice. *Stud. Surf. Sci. Catal.*; Van Bekkum, H., Flanigen, E. M., Eds.; **1991**, *58*, 285.
(4) Wu, Y.; Chmelka, B. F.; Pines, A.; Davis, M. E.; Grobet, P. J.; Jacobs, P. A. *Nature* **1990**, *346*, 550. Jelinek, R.; Chmelka, B. F.; Wu, Y.; Grandinetti, P. J.; Pines, A.; Barrie, P. J.; Klinowski, J. *J. Am. Chem. Soc.* **1991**, *113*, 4097.
(5) NMR experiments were recorded in a 11.7 T magnetic field on a Chemagnetics CMX-500 spectrometer. The DOR experiments were carried out with a home-built DOR probe whose features have been described elsewhere.[7] A total of 3000–5000 acquisitions were accumulated, using short radio frequency pulses with 0.5-s delays. The external reference used was 0.1 M NaCl.
(6) McMurray, L.; Holmes, A. J.; Kuperman, A.; Ozin, G. A.; Özkar, S. *J. Phys. Chem.* **1991**, *95*, 9448.
(7) Wu, Y.; Sun, B. Q.; Pines, A.; Samoson, A.; Lippmaa, E. *J. Magn. Reson.* **1990**, *89*, 297.
(8) Özkar, S.; Ozin, G. A.; Moller, K.; Bein, T. *J. Am. Chem. Soc.* **1990**, *112*, 9575. Jelinek, R.; Özkar, S.; Ozin, G. A. *J. Phys. Chem.*, in press.
(9) Fitch, A. M.; Jobic, H.; Renouprez, A. *J. Phys. Chem.* **1986**, *90*, 1311.

0002-7863/92/1514-4907$03.00/0